crystals

MDPI

Communication

Characteristics of Flakes Stacked Cr_2N with Many Domains in Super Duplex Stainless Steel

Po-Chiang Lin [1], Yu-Ting Tsai [2], Neng-Hao Gan [1], Jer-Ren Yang [2], Shing-Hoa Wang [1,*], Horng-Yi Chang [3], Tzy-Rong Lin [1] and Po-Kai Chiu [4]

1 Department of Mechanical and Mechatronic Engineering, National Taiwan Ocean University, Keelung 20224, Taiwan; j2034457@hotmail.com.tw (P.-C.L.); 10772041@email.ntou.edu.tw (N.-H.G.); trlin@mail.ntou.edu.tw (T.-R.L.)

2 Department of Materials Science and Engineering, National Taiwan University, Taipei 10617, Taiwan; f99527004@ntu.edu.tw (Y.-T.T.); jryang@ntu.edu.tw (J.-R.Y.)

3 Department of Marine Engineering, National Taiwan Ocean University, Keelung 20224, Taiwan; hychang@ntou.edu.tw

4 Taiwan Instrument Research Institute, National Applied Research Laboratories, Hsinchu 30076, Taiwan; pkchiu@tiri.narl.org.tw

* Correspondence: shwang@email.ntou.edu.tw

Received: 26 September 2020; Accepted: 22 October 2020; Published: 24 October 2020

Abstract: This study mainly observed the Cr_2N (chromium nitride) nucleation and growth in SAF 2507 duplex stainless steel. However, the investigation revealed that Cr_2N has a complex substructure separated into many regions. In SAF 2507 duplex stainless steel, Cr_2N nucleated at the dislocations and the precipitates were composed of many Cr_2N flakes gathered together when aged at 600 °C.

Keywords: super duplex stainless steel; chromium nitride; dislocation

1. Introductions

Duplex stainless steels (DSS) have been widely used as structural materials in the power, chemical and oil industries [1–3]. The beneficial mixture of austenitic (γ) and ferritic (δ) properties in the duplex microstructure ($\delta + \gamma$) results in high strength with desirable toughness [4], combined with a good corrosion resistance, especially against chloride-induced pitting and crevice corrosion, as well as stress corrosion cracking [5–7]. The heat treated SAF 2507 DSS can lead to a series of transformations in the ferrite matrix or at the interphase boundaries, in addition to the martensite forms from the austenite [8,9]. In a previous study [10], the different new phases and precipitates of the δ-ferrite matrix decomposition were characterized in the temperature range of 400–1050 °C. The phase transformation in DSS always takes place in ferrite rather than in austenite for two reasons. First, the atomic density is lower in the lattice of ferrite than in the lattice of austenite; second, the enriched chromium (Cr) and molybdenum (Mo) in the ferrite phase is favorable for interphase nucleation [10]. The characterization of the phase precipitates is best performed on isothermally heat-treated samples with a fully δ-ferrite microstructure retained by water quenching to room temperature. This isothermal treatment induces the decomposition of the supersaturated δ-ferrite and produces various phases: $M_{23}C_6$ and M_7C_3 carbides [8], secondary austenite formed as Widmannstätten precipitates [11], δ-ferrite decomposed to secondary austenite (γ_2) with σ phases via the eutectoid reaction [12,13], τ phase [14], R phase [15], σ phase [16,17] and chi (χ) [17,18] phase. The intermetallic χ-phase, whose characterization is reported in the present paper, is a tetrahedral close-packed (TCP) phase.

The presence of this phase was reported for the first time by Andrews and Brookes [19] in a steel containing Cr, Ni and Mo. McMullin et al. [20] have also found the presence of an equilibrium phase of this intermetallic compound in the temperature range of 815–900 °C as isothermal sections of the

ternary diagram for Fe-Cr-Mo. Intermetallic phases (χ and σ) and Cr_2N precipitate in grains or at phase boundaries during slow cooling in the critical temperature range of 1000 °C (1273 K) to 700 °C (973 K). Another aspect is that a high density of chromium nitrides is generated in the interior of the ferrite grains as a result of super-saturation with nitrogen by rapid cooling from high temperatures by quenching [21]. As the nitrogen solubility in ferrite is quite low, it leads a super-saturation of nitrogen in ferrite [22].

A stimulating effect on sigma phase precipitation in DSS can be achieved by cold working prior to aging. The microstructures in deformed steels, similar to the un-deformed steels, exhibit the transformation of ferrite phase into a mixture of secondary austenite and sigma phase [23,24]. In the meantime, its amount is increased by the nitrogen content [25]. The nucleation sites of sigma are the incoherent twin boundaries, grain boundaries and the intra-granular dislocations [26]. Accidentally, it also nucleates at coherent twin boundaries [23]. A key point to point out is that Cr_2N is found in the range of 700–900 °C, somewhat lower temperatures, whereas σ phase forms essentially in the temperature range of 800–1010 °C. Another remarkable feature is the intermetallic R phase precipitates after aging at 700 °C for 3 h, but dissolves after longer aging times, the intermetallic R phase was not observed after 72 h and no evidence of any carbides of any different type was found [26]. The substantial amounts of N caused the grain boundary Cr_2N, which often formed in cooperation with secondary austenite [26]. As δ-ferrite decomposes to σ and γ_2 phases, Cr migrates to the σ phase and N is absorbed by the γ_2 phase via the eutectoid decomposition process. After a certain duration of aging, the δ-ferrite completely decomposes, causing the growth of σ phase to stop. Finally, the positions of primary δ-ferrite are collectively occupied by the σ and γ_2 phases [27].

The Cr_2N epsilon phase co-exists along with secondary austenite and the sigma phase at temperatures below 950 °C. The literature of TEM studies have revealed the two morphologies of inter-granular and intra-granular Cr_2N precipitates. Ductility deteriorates with a rise in yield strength simultaneously as the aging time increases [28]. In the meantime, it has a reduction in the toughness and corrosion properties too [29]. Particularly at 475 °C, with aging times greater than 17 h, this aging treatment at low temperature can cause a significant reduction in the impact strength and toughness of DSS 2205 [30]. Precipitates of Cr_2N exist at δ/δ, δ/γ phase boundaries and within the δ ferrite matrix after water quenching from a high solution temperature. Nevertheless, these Cr_2Ns in the form of lath-shaped crystals are distributed at the δ ferrite sub-grain boundaries [31].

From the preceding welding study [32], there were many Cr_2N precipitates found in the δ ferrite of super DSS. This gives rise to the motivation to investigate the nucleation and growth of the Cr_2N microstructural evolution in its early stage for this super DSS during aging. At present, no report discloses details of the mechanism of Cr_2N nucleation and growth.

2. Materials and Methods

Fe-0.01C-0.37Si-0.65Mn-23.9Cr-6.53Ni-0.19Co-3.74Mo-0.31Cu-0.03N in wt.% is the chemical composition of SAF 2507 DSS as determined with a glow discharge spectrometer (GDS). The samples were heated at 750 °C with a holding time of 5 h, or at 600 °C with holding times in a series of 5, 10, 30, 60, 90 min, and 7 h, respectively, then they were water quenched after aging.

The foils examined under the transmission electron microscope (TEM) in a model of FEI Tecnai G2 F30 were prepared using the following procedure: the specimens were thinned to a thickness of 0.2 mm with #400 sandpaper and further thinned to 0.1 mm with #800 sandpaper before being electro-polished with a twin jet at 45 V in a solution of 5% perchlorate, 25% glycerin, and 70% ethyl alcohol at −5 to −10 °C. Punched 3-mm diameter disks were further thinned to 0.05 mm with #1200 sandpaper.

3. Results and Discussion

3.1. Cr_2N Transformation at 600 °C under 7 h Holding in SAF 2507

The microstructural details of Cr_2N precipitation in δ ferrite were investigated by transmission electron microscopy (TEM). Two typical shapes of coarse Cr_2N precipitates were revealed in Figure 1, the precipitates at the phase boundary were mostly needle shapes with a particular crystal orientation relationship (OR) to the matrix and the others were within the grains after the relatively long time of aging of 7 h at 600 °C. Cr_2N dispersedly precipitated within the δ ferrite in specimens aged at 600 °C for 7 h. The selected-area diffraction patterns, which were obtained from the interfacial regions of the Cr_2N and δ phase, as shown in Figure 1, indicated a characteristic orientation relationship between Cr_2N and the δ phase. A dispersion of finer precipitates of Cr_2N existed within the δ ferrite grain, although coarser nitrides are distributed mainly as stacks along the ferrite sub-grain boundaries. It seemed that the favored heterogeneous nucleation at sub-grain boundaries or dislocations determined the variation in nitride size [33].

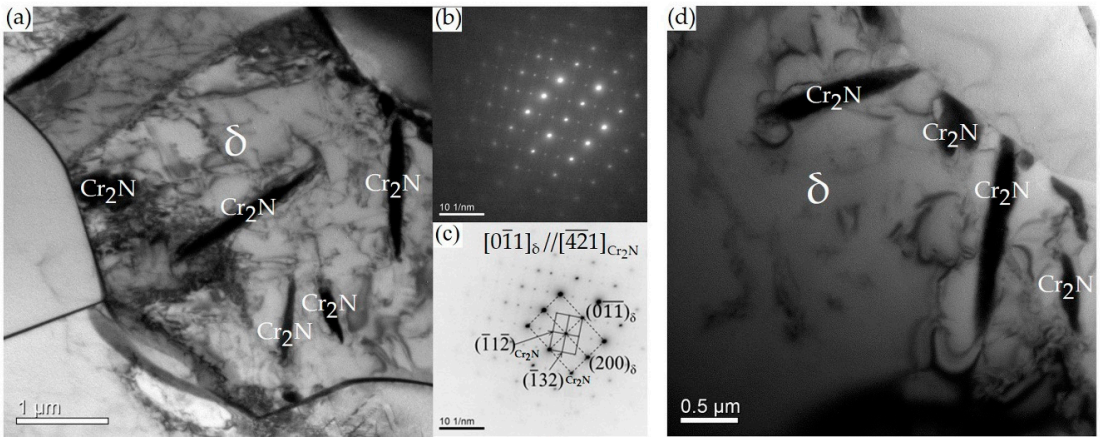

Figure 1. Microstructure of a specimen aged at 600 °C for 7 h (**a**) transmission electron micrograph showing Cr_2N precipitated within δ-ferrite; (**b**) diffraction pattern with zone $\left[0\bar{1}1\right]_{\delta}\left\|\left[\bar{4}\bar{2}1\right]_{Cr_2N}\right.$; (**c**) interpretation of (**b**); (**d**) Cr_2N formed at phase boundary.

3.2. The Detailed Substructure of Cr_2N

Figure 2a is a micrograph of Cr_2N precipitated at 600 °C after 7 h holding, and Figure 2b presents a high magnification image of Figure 2a. Figure 2c is the micrograph of Cr_2N precipitated at 750 °C after 5 h holding, and Figure 2d presents a high magnification image of Figure 2c. What is interesting is that Cr_2N in the high magnification images has many fringes in it (Figure 2b), and even two fringe directions can be observed (Figure 2d). The substructure within Cr_2N is visible. Furthermore, the further high magnification of Cr_2N precipitated at 750 °C after 5 h of holding shows that Cr_2N is not as simple as we have seen. The fact is that Cr_2N is composed of many different domains (Figure 3a), which are further separated into different regions, as illustrated by the HRTEM or HREM (High-resolution transmission electron microscopy) image (Figure 3b).

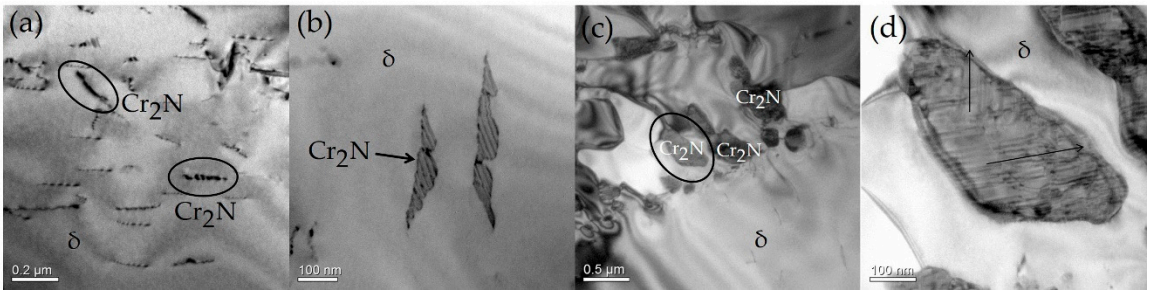

Figure 2. (**a**) TEM micrograph of a specimen aged at 600 °C for 7 h, and (**b**) high magnification of (**a**); (**c**) TEM micrograph of a specimen aged at 750 °C for 5 h, and (**d**) high magnification of (**c**), showing the many fringes in Cr_2N.

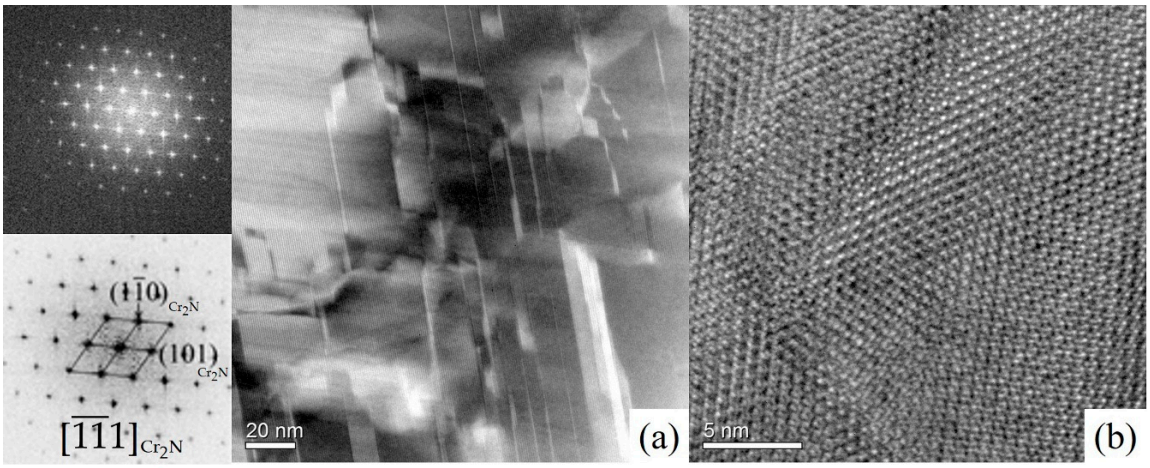

Figure 3. (**a**) TEM micrograph showing the substructure of Cr_2N (**b**) HRTEM image recorded along the $\left[\overline{1}11\right]$ zone axis showing that Cr_2N has a complex microstructure characterized by separation into different regions.

3.3. Nucleation and Growth Mechanism of Cr_2N at 600 °C

Although the metastable Cr_2N exhibited a needle-like shape in Figure 1, a detailed examination showed that the nucleation of the Cr_2N at 600 °C consisted of several small flakes in a particular arrangement in Figure 3. In order to display Cr_2N nucleation very clearly, the dark-field images (DFI) in Figure 4c–h were utilized by tilting the sample until it satisfied the invisible condition of **g** vector dot burger vector **b** equal to zero ($\mathbf{g} \cdot \mathbf{b} = 0$), to eliminate the most dislocations, as the size of nucleated Cr_2N was too small and thin to obtain diffraction spots. The sequence of Cr_2N nucleation, growth and coalescence is shown in Figure 4a–i. Cr_2N nucleated at the dislocations appeared as stacks of several small flakes in parallel (Figure 4g,h) or two mutually perpendicular flakes (Figure 4f). To clarify the mechanism of Cr_2N nucleation and growth in the δ phase of DSS, SAF 2507 was heated to 600 °C for different aging times. At 600 °C, the dislocations appeared in the δ phase after 5 min (Figure 4a). The tiny Cr_2N nucleated at the dislocations after 10 min (Figure 4b,c). After 30 min of holding, Cr_2N gradually grew into flakes, and a large amount of Cr_2N flakes were distributed within the α matrix (Figure 4d–h). Finally, after 7 h, Cr_2N flakes stacked together to form needle-like Cr_2N (Figure 4i). It is notable that the two directions of Cr_2N flake growth were along the $\left(0\overline{2}0\right)$ plane and the $\left(00\overline{2}\right)$ plane, and the Burgers vector of the dislocation loops, which were tangled with the Cr_2N flakes, was $1/2 < 111 >$, as shown in Figure 4e. During rapid cooling from the δ ferrite field, the microstructure consisted of large ferrite grains with a low amount of allotriomorphic and Widmanstätten austenite and abundant intra-granular nitrides [34]. These Cr_2N rods or CrN plates followed a kinetic "C" curve to precipitate from the ferrite by nucleation and growth [34]. Dislocations, inclusions, grain boundaries

(δ/δ), and interphase interfaces (δ/γ) were the locations for nucleation of Cr_2N rods. The corrosion resistance and toughness of DSSs were sacrificed severely by the Cr_2N precipitation [34].

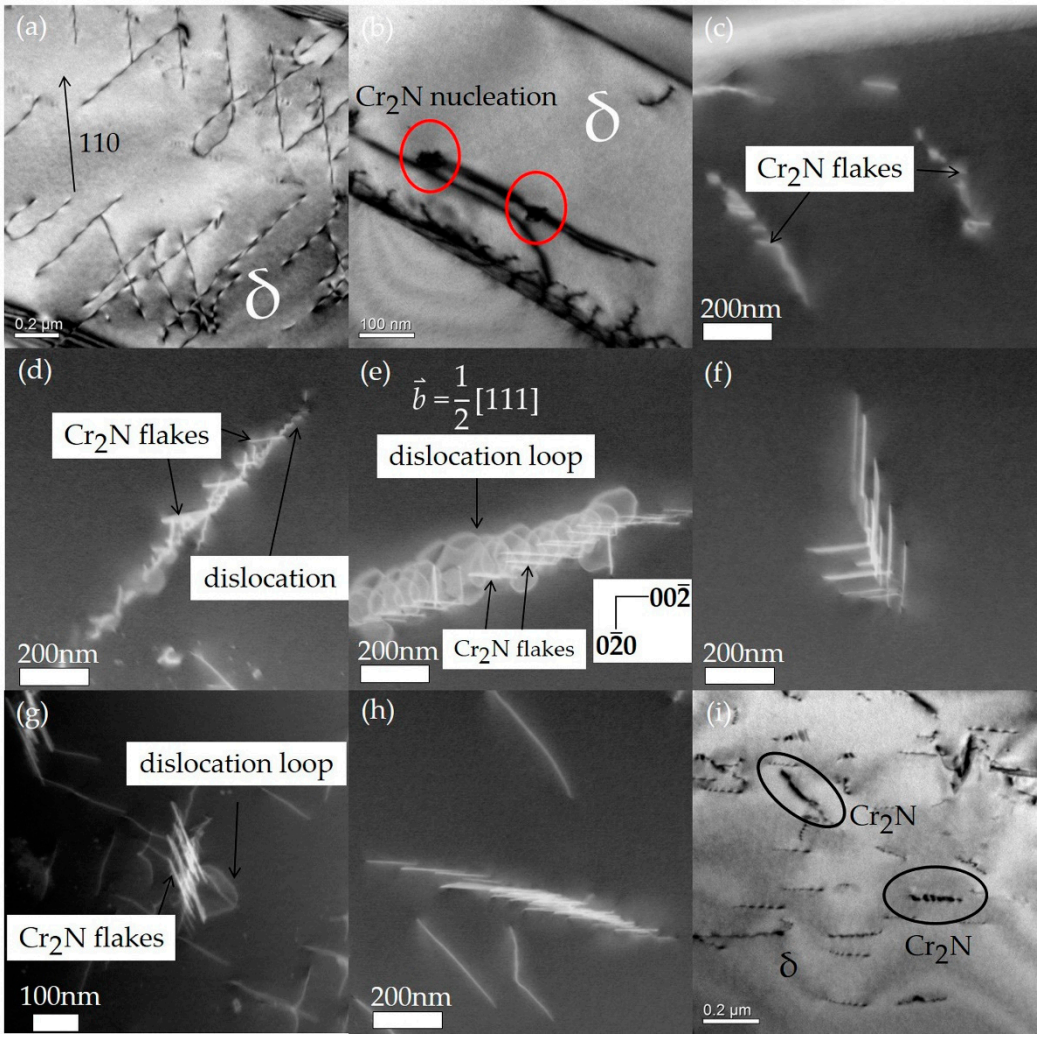

Figure 4. The sequence of the Cr_2N nucleation and growth mechanism at 600 °C. (**a**) 5 min for only lattice defects of dislocation, (**b**,**c**) 10 min for Cr_2N nucleated at dislocations, (**d**–**h**) 30 min for Cr_2N flakes either stacked mutually perpendicular or stacked parallel together, (**i**) 7 h for Cr_2N flakes coalescence.

4. Conclusions

There are two morphologies for Cr_2N nucleation and growth. One precipitation occurs at grain or phase boundary and forms the micrometric size Cr_2N that are mostly needle shapes with a particular crystal orientation relationship (OR) to the matrix. Another precipitation occurs within the matrix and forms the nanometric size Cr_2N composed of flakes, or of many orientation domains. Cr_2N first nucleated in multiple positions at dislocations and gradually grew into many flakes, which grew in perpendicular or in parallel. Furthermore, the Cr_2N flakes interacted with dislocation loops. At longer holding times, dislocations were discharged and the Cr_2N finally coalesced and eventually grew into complete needle-like Cr_2N with many domains.

Author Contributions: Investigation, methodology, writing—original draft, formal analysis, P.-C.L.; methodology, data curation, validation, Y.-T.T.; writing—original draft, visualization, N.-H.G.; conceptualization, writing—review and editing, project administration, funding acquisition, supervision, S.-H.W.; conceptualization, writing—review and editing, J.-R.Y.; conceptualization, H.-Y.C.; resources, conceptualization, T.-R.L.; resources, visualization, P.-K.C. All authors have read and agreed to the published version of the manuscript.

Funding: This research was financial supported by the Ministry of Science and Technology (MOST) of Taiwan under the grant MOST 109-2221-E-019-047.

Conflicts of Interest: No conflict of interest is declared by all authors.

References

1. Davision, R.M.; Redmond, J.D. Practical guide to using duplex stainless steels. *Mater. Perform.* **1990**, *29*, 57–62.
2. Kiesheyer, H. *Proceedings of the International Conference on Stainless Steels'91*; The Iron and Steel Institute of Japan: Chiba, Japan, 1991; p. 1148.
3. Fruytier, D.J. Industrial experiences with duplex stainless steel related to their specific properties. *Duplex Stainl. Steels* **1991**, *1*, 497–509.
4. Foct, J.; Akdut, N.; Gottstein, G. Why are "duplex" microstructures easier to form than expected? *Scr. Metall. Mater.* **1992**, *27*, 1033–1038. [CrossRef]
5. Sridhar, N.; Kolts, J.; Flasche, L.H. A duplex stainless steel for chloride environments. *JOM* **1985**, *37*, 31–35. [CrossRef]
6. Magnin, T.; Lardon, J.M. Cyclic deformation mechanisms of a two-phase stainless steel in various environmental conditions. *Mater. Sci. Eng. A* **1988**, *104*, 21–28. [CrossRef]
7. Bernhardsson, S.; Oredsson, J.; Martenson, C. *Duplex Stainless Steels*; American Society for Metals: Metals Park, OH, USA, 1983; p. 267.
8. Solomon, H.D.; Devine, T.M., Jr. *Duplex Stainless Steels—A Tale of Two Phases*; American Society for Metals: Metals Park, OH, USA, 1982; pp. 693–756.
9. Örnek, C.; Zhong, X.; Engelberg, D.L. Low-Temperature environmentally assisted cracking of grade 2205 duplex stainless steel beneath a $MgCl_2$: $FeCl_3$ salt droplet. *Corrosion* **2016**, *72*, 384–399. [CrossRef]
10. Nilsson, J.O. Super duplex stainless steels. *Mater. Sci. Technol.* **1992**, *8*, 685–700. [CrossRef]
11. Ohmori, Y.; Nakai, K.; Ohtsubo, H.; Isshiki, Y. Mechanism of Widmanstätten austenite formation in a δ/γ duplex phase stainless steel. *ISIJ Int.* **1995**, *35*, 969–975. [CrossRef]
12. Shek, C.H.; Shen, G.J.; Lai, J.K.L.; Duggan, B.J. Early stages of decomposition of ferrite in duplex stainless steel. *Mater. Sci. Technol.* **1994**, *10*, 306–311. [CrossRef]
13. Chen, T.H.; Yang, J.R. Effects of solution treatment and continuous cooling on σ-phase precipitation in a 2205 duplex stainless steel. *Mater. Sci. Eng. A* **2001**, *311*, 28–41. [CrossRef]
14. Redjaimia, A.; Ruterana, P.; Metauer, G.; Gantois, M. Identification and characterization of a novel intermetallic compound in a Fe-22 wt% Cr-5 wt% Ni-3 wt% Mo-0.03 wt% C duplex stainless steel. *Philos. Mag. A* **1993**, *67*, 1277–1286. [CrossRef]
15. Redjaïmia, A.; Morniroli, J.P.; Donnadieu, P.; Metauer, G. Microstructural and analytical study of heavily faulted Frank-Kasper R-phase precipitates in the ferrite of a duplex stainless steel. *J. Mater. Sci.* **2002**, *37*, 4079–4091. [CrossRef]
16. Martins, M.; Casteletti, L.C. Sigma phase morphologies in cast and aged super duplex stainless steel. *Mater. Charact.* **2009**, *60*, 792–795. [CrossRef]
17. Ghosh, S.K.; Mondal, S. High temperature ageing behaviour of a duplex stainless steel. *Mater. Charact.* **2008**, *59*, 1776–1783. [CrossRef]
18. Escriba, D.M.; Materna-Morris, E.; Plaut, R.L.; Padilha, A.F. Chi-phase precipitation in a duplex stainless steel. *Mater. Charact.* **2009**, *60*, 1214–1219. [CrossRef]
19. Andrews, K.W.; Brookes, P.E. Chi Phase in Alloy Steels. *Met. Treat. Drop Forg.* **1951**, *18*, 301.
20. McMullin, J.G.; Reiter, S.F.; Ebeling, D.G. Equilibrium Structures in Fe-Cr-Mo Alloys. *Trans. Am. Soc. Met.* **1954**, *46*, 799–811.
21. Pettersson, N.H.; Lindell, D.; Lindberg, F.; Borgenstam, A. Formation of Chromium Nitride and Intragranular Austenite in a Super Duplex Stainless Steel. *Metall. Mater. Trans. A* **2019**, *50*, 5594–5601. [CrossRef]
22. Muthupandi, V.; Srinivasan, P.B.; Seshadri, S.; Sundaresan, S. Effect of weld metal chemistry and heat input on the structure and properties of duplex stainless steel welds. *Mater. Sci. Eng. A* **2003**, *358*, 9–16. [CrossRef]
23. Weiss, B.F.; Stickler, R. Phase instabilities during high temperature exposure of 316 austenitic stainless steel. *Metall. Mater. Trans. B* **1972**, *3*, 851–866. [CrossRef]

24. Cho, H.S.; Lee, K. Effect of cold working and isothermal aging on the precipitation of sigma phase in 2205 duplex stainless steel. *Mater. Charact.* **2013**, *75*, 29–34. [CrossRef]
25. Oh, Y.J.; Hong, J.H. Nitrogen effect on precipitation and sensitization in cold-worked Type 316L (N) stainless steels. *J. Nucl. Mater.* **2000**, *278*, 242–250. [CrossRef]
26. Nilsson, J.O.; Wilson, A. Influence of isothermal phase transformations on toughness and pitting corrosion of super duplex stainless steel SAF 2507. *Mater. Sci. Technol.* **1993**, *9*, 545–554. [CrossRef]
27. Zhang, B.; Jiang, Z.; Li, H.; Zhang, S.; Feng, H.; Li, H. Precipitation behavior and phase transformation of hyper duplex stainless steel UNS S32707 at nose temperature. *Mater. Charact.* **2017**, *129*, 31–39. [CrossRef]
28. Mishra, M.K.; Rao, A.G.; Sarkar, R.; Kashyap, B.P.; Prabhu, N. Effect of preaging deformation on aging characteristics of 2507 super duplex stainless steel. *J. Mater. Eng. Perform.* **2016**, *25*, 374–381. [CrossRef]
29. Nilsson, J.O.; Wilson, A.; Josefsson, B.; Thorvaldsson, T. Relationship between pitting corrosion, toughness and microstructure for isothermally heat treated super duplex stainless steel. *Appl. Stainl. Steel* **1992**, *1*, 280–289.
30. Simmons, J.W. Overview: High-nitrogen alloying of stainless steels. *Mater. Sci. Eng. A* **1996**, *207*, 159–169. [CrossRef]
31. Lin, K.; Shi, H.Q.; Ma, L.Q.; Ding, Y. The Analysis and Research of Secondary Phases Generated during Isothermal Aging of Duplex Stainless Steels. *Appl. Mech. Mater.* **2012**, *193–194*, 411–417. [CrossRef]
32. Tsai, Y.-T.; Lin, P.-C.; Chen, Y.-W.; Wang, S.-H.; Yang, J.-R. Fatigue behavior and microstructural characteristics of a duplex stainless steel weld metal under vibration-assisted welding. *Mater. Sci. Eng. A* **2018**, *721*, 319–327. [CrossRef]
33. Pettersson, N.; Pettersson, R.F.; Wessman, S. Precipitation of chromium nitrides in the super duplex stainless steel 2507. *Metall. Mater. Trans. A* **2015**, *46*, 1062–1072. [CrossRef]
34. Ramirez, A.J.; Lippold, J.C.; Brandi, S.D. The relationship between chromium nitride and secondary austenite precipitation in duplex stainless steels. *Metall. Mater. Trans. A* **2003**, *34*, 1575–1597. [CrossRef]